

Exploring a Model of a Chemokine Receptor/Ligand Complex in an Explicit Membrane Environment by Molecular Dynamics Simulation: The Human CCR1 Receptor

Mohsen Shahlaei,^{†,‡} Armin Madadkar-Sobhani,^{§,||} Afshin Fassihi,^{*,†} and Lotfollah Saghraie[†]

[†]Department of Medicinal Chemistry, School of Pharmacy and Pharmaceutical Sciences, Isfahan University of Medical Sciences, 81746-73461, Isfahan, Iran

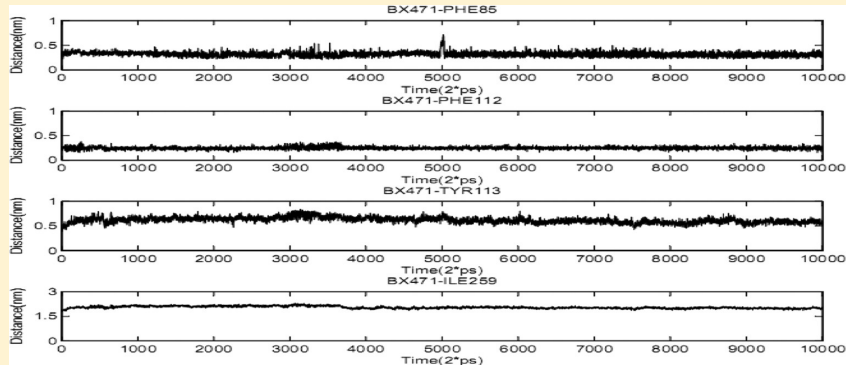
[‡]Department of Medicinal Chemistry, School of Pharmacy and Pharmaceutical Sciences, Kermanshah University of Medical Sciences, Kermanshah, Iran

[§]Department of Life Sciences, Barcelona Supercomputing Center, C\ Jordi Girona 31, Edificio Nexus II, 08028 Barcelona, Spain

^{||}Department of Bioinformatics, Institute of Biochemistry and Biophysics, University of Tehran, Tehran, Iran

 Supporting Information

ABSTRACT:



The seven transmembrane helices G-protein-coupled receptors (GPCRs) form one of the largest superfamilies of signaling proteins found in humans. Homology modeling, molecular docking, and molecular dynamics (MD) simulation were carried out to construct a reliable model for CCR1 as one of the GPCRs and to explore the structural features and the binding mechanism of BX471 as one of the most potent CCR1 inhibitors. In this study, BX471 has been docked into the active site of the CCR1 protein. After docking, one 20 ns MD simulation was performed on the CCR1-ligand complex to explore effects of the presence of lipid membrane in the vicinity of the CCR1-ligand complex. At the end of the MD simulation, a change in the position and orientation of the ligand in the binding site was observed. This important observation indicated that the application of MD simulation after docking of ligands is useful. Explorative runs of molecular dynamics simulation on the receptor–ligand complex revealed that except for Phe85, Phe112, Tyr113, and Ile259, the rest of the residues in the active site determined by docking are changed. The results obtained are in good agreement with most of the experimental data reported by others. Our results show that molecular modeling and rational drug design for chemokine targets is a possible approach.

1. INTRODUCTION

Chemokines are a well-known group of proteins that have an important role in leukocyte activation and migration.¹ Chemokines CCL3 (MIP-1 α) and CCL5 (RANTES) attach to their common receptor CCR1, which is expressed on a number of human cell types such as monocytes, macrophages, dendritic, and T cells. A large number of reports have been published about the chemokine receptor CCR1 and its major ligands to the pathogenesis of chronic inflammatory diseases including rheumatoid arthritis,² multiple sclerosis,³ and transplant rejection.⁴ This has illustrated the therapeutic potential of CCR1 antagonists in the treatment of such diseases and thus made CCR1 an attractive target for drug discovery research.^{5,6}

CCR1 belongs to the G-protein coupled receptors (GPCRs), one of the well-known and well studied superfamilies of bio-membrane proteins.⁷

Due to their extensive distribution among different body tissues, their participation in several biochemical pathways, together with their exposition to the extracellular environment, GPCRs are the most important macromolecular target class of macromolecules for the drug development process.⁸

Yet, to be used in pharmacology and particularly in structure based drug design, the structure of the target protein must be

Received: June 13, 2011

Published: September 12, 2011

Table 1. Prediction of Transmembrane Regions of CCR1 by Various Methodologies

method	no. of TM	TM1 Cter.-Nter.	TM2 Cter.-Nter.	TM3 Cter.-Nter.	TM4 Cter.-Nter.	TM5 Cter.-Nter.	TM6 Cter.-Nter.	TM7 Cter.-Nter.
HMMTOP	7	36–60	69–91	107–129	147–172	203–227	240–264	281–305
DAS	6	38–61	72–90	117–142	147–166	203–224	238–265	
mobyle	7	40–60	71–91	109–129	146–166	203–223	237–257	285–305
PORTER	7	31–61	68–96	103–135	147–170	196–228	234–264	279–317
SABLE	7	29–61	68–95	103–141	151–172	191–228	240–266	275–318
SPLIT	7	38–61	69–90	116–142	146–169	203–226	238–266	282–305
TMHMM	7	37–59	71–93	108–127	147–169	205–227	240–262	282–304
TMpred	7	43–59	72–91	108–129	147–171	203–223	237–255	285–304
SOSUI	6	36–58	69–91	120–142	148–169	202–224	242–264	
TMmod	7	40–60	71–91	111–135	147–171	205–227	240–264	284–304
PolyPhobius	7	40–60	72–91	112–134	147–170	203–226	238–261	284–304

known to a high level of confidence. This is typically provided by the X-ray crystallography procedure. Up to now, attaining a high-resolution structure is a particularly complicated achievement when working with membrane proteins, whose crystallization does not take place as simply as aqueous proteins. The lipid environment in the membrane has an obvious effect on the conformation of the membrane protein,⁹ and hence compared with the large number of known aqueous protein structures, structural details of very few membrane proteins is available. One of the most important approaches to overcome this deficiency is the use of computational methods. Determination of the 3D structure of some GPCRs by experimental methods^{10–13} has opened the way for computational modeling studies of these proteins.

Computational methods such as molecular dynamics simulation and docking are powerful tools at the molecular level for understanding the mechanism of action of drugs. Our interest in the blockage mechanism of chemokine receptors as a member of GPCRs especially CCR1 stems from our efforts to design new chemokine antagonists.^{6,14,15} However, no experimental data about the detailed molecular structure of ligand-CCR1 complexes have been reported yet. It must be noted that computational methods may reveal data which are not easy to obtain by experiments.¹⁶ Recently, great achievement has been attained in the field of molecular modeling and structure prediction of chemokine receptors, because the structure of CXCR4, one of the members of this receptors, has been resolved.¹⁷ The molecular dynamics simulation procedure provides a great deal of useful data about the stability of noncovalent interactions in water and lipid membrane and the mobility of the amino acid residues within the protein frame. MD simulations could be employed to simulate the binding process of ligand(s) to the active site of protein(s), to discover the binding conformation, and to explore the protein binding mechanism of ligand at molecular and atomic levels. This kind of calculations has a benefit of iteratively tracking the trajectory of conformational changes.

BX471 is a small-molecule CCR1 antagonist which is currently in phase II of clinical trials.¹⁸ It is a piperazine-based molecule which is able to displace natural CCR1 ligands MIP-1 α , RANTES, and MCP-3 with a high affinity ($K_i = 1\text{ nM}$ to 5.5 nM).¹⁹ BX471 has been widely studied in a spectrum of animal models and in a human clinical trial.²⁰ Therefore, this molecule is selected for more consideration as a representative of CCR1 antagonists. Although BX471 has shown excellent potency in human CCR1 binding as well as exhibiting selectivity against other CCRs, detailed binding mechanism has not been studied in the literature for this compound. All this prompts us to perform a

computational molecular modeling study on CCR1 to investigate the mechanism of action of BX471.

To the best of our knowledge, no 3D structure of CCR1 was constructed, and no MD simulation has been performed so far on this protein.

For these purposes, at first, we have carried out a 20 ns MD simulation of the developed model in lipid biomembrane, and after obtaining a stable model of protein, we scanned the binding site using the docking computational protocol to identify the binding mode of BX471. An extra MD simulation was performed on CCR1 in the presence of its antagonist in lipid biomembrane.

Previous experimental studies demonstrate that different binding interactions of ligands to a receptor lead to different receptor conformations.²¹ Thus, we faced two challenges: (1) how to construct the 3D models of CCR1 receptor and (2) how to identify the binding conformations of the receptor in complex with the ligand. To circumvent these difficulties, several modeling and simulation approaches were utilized in this study.

Here, we are going to further develop our knowledge about the binding of BX471 to CCR1, in a manner similar to the previous work of our group on CCR5.¹⁵

In this study, thanks to modern software and hardware, one of the most important goals is to investigate the effects of lipid bilayer on the dynamical behavior of the developed CCR1 model.

Other objectives of the present study are (i) to demonstrate the common binding mode of BX471 with CCR1; (ii) to explain the structural characteristics required for the binding of CCR1 antagonists to the receptor; and (iii) to obtain a stable and reliable 3D model of CCR1 representing the main structural features of this protein, which can be employed in proposing more selective and more potent CCR1 antagonists.

On the other hand, in the present research, we are also going to report, to the best of our knowledge, one of the first modeling studies that uses CXCR4 as a template to model a chemokine receptor.

2. METHODS

2.1. Template Searching, Transmembrane Helix Prediction, and Homology Modeling. The primary sequences of human CCR1 were obtained from Swiss-Prot database (Accession number P32246). Blastp (Basic Local Alignment Search Tool) at the NCBI was used to find the homologous proteins with known structures to be employed as the template in the process of CCR1 homology modeling.²² The crystal structure of the CXCR4 receptor (PDB ID: 3ODU) at 2.50 Å resolution was selected

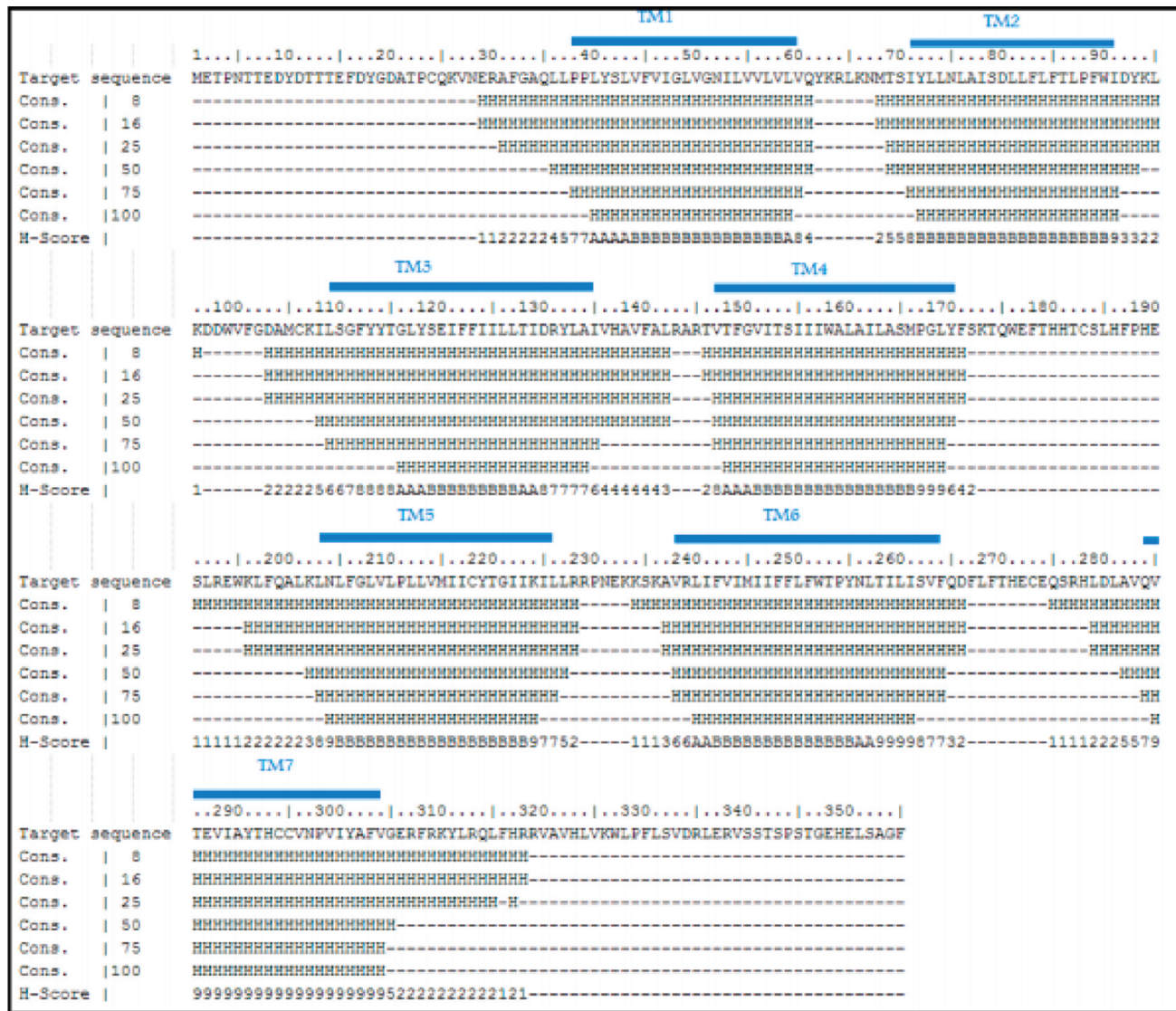


Figure 1. Consensus of 8, 16, 25, 50, 75, 90, and 100% of each residue in CCR1 predicted as helix by 11 different helix prediction methods. Each residue has a H-Score from 1 to 11 based on how many methods predicted it as helix. A and B in scoring scale are equal to 10 and 11. Consensus 50% comprises residues which have 6 or more scores.

as the modeling template of CCR1 and obtained from the protein data bank.¹⁷ Transmembrane prediction of proteins is not an easy task,²³ due to the limited set of information available to evaluate the methods.²⁴ To model the topology of CCR1, 11 different topology prediction techniques were employed, including DAS,²⁵ HMMTOP,²⁶ SOSUI,²⁷ TMHMM,²⁸ TMMOD,²⁹ TMpred,³⁰ SPLIT,³¹ SABLE,³² PORTER,³³ PolyPhobius,³⁴ and mobyle pateur.³⁵ All methods were used in single sequence mode, and all user adjustable parameters were left at their default values.

After predicting helices by these servers, a consensus approach was employed. In this method for each residue a consensus prediction was calculated by counting the number of servers that predicted the residue as being in α -helix. For example consensus 100% was assigned to a residue which was predicted as α -helix by all of the 11 methodologies. The same procedure was used to predict TM helices of CXCR4.

On the other hand, the secondary structure of the CXCR4 was analyzed by DSSP.³⁶

Table 1 summarizes the obtained prediction results of the number of helices and their locations in CCR1 sequence. Consensus 8%, 16%, 25%, 50%, 75%, and 100% of applied methods which predict α -helices for the sequence are assigned and shown in Figure 1. The 50% consensus for the CXCR4 was almost well-suited with DSSP assignment and hence was selected for assessment of helices predicted in the constructed model.

In the homology modeling step, we would like to look for an experimentally determined structure of high sequence identity with a CCR1 receptor. To align the sequence of the human CCR1 receptor with that of CXCR4, the CLUSTALW program was employed directly from its Web site at <http://www2.ebi.ac.uk/CLUSTALW>.³⁷ The alignment was edited manually based on the results of TM helix prediction procedure and conserved key residues of GPCRs reported by Baldwin et al.³⁸

The obtained alignment is provided in Figure S1 in the Supporting Information.

MODELER 9v2³⁹ was used to build homology models of CCR1 from the CXCR4 crystallographic structure. From the

alignment, 3D models containing all non-hydrogen atoms were obtained automatically using the method implemented in MODELER. 1000 conformations of CCR1 receptor were generated, among, the one corresponding to the lowest value of the probability density function (pdf) and the fewest restraints violations was used for further analysis. An *ab initio* method implemented in the MODELER that has been demonstrated to be able to predict the conformations of loop regions was used to build some loops of the best model.

The root-mean-square deviations (*rmsds*) of the models relative to template were calculated using MODELER.

The overall stereochemical quality of the final selected model for CCR1 was accessed by the program PROCHECK.⁴⁰ Environment profile of the final developed model was checked using verify-3D (Structure Evaluation Server).⁴¹

2.2. Docking. The geometry of BX471 ligand was constructed based on its structure¹⁸ and optimized at the DFT/B3LYP/6-311G** level (Figure S2). The optimized structure was saved as a PDB file and transferred into linux environment to perform docking procedure.

Docking simulations were carried out using the AutoDock program (v.4.0).⁴² Grid maps of $70 \times 70 \times 70 \text{ \AA}$ representing the protein were calculated with AUTOGRID and a grid-point spacing of 0.375 \AA (roughly a quarter of the length of a carbon–carbon single bond) was applied; such maps were centered on the atom C_{α} of Tyr113. Of the three different search algorithms offered by AutoDock4, the LGA approach was used for the global optimum binding position search.

Schematic two-dimensional representations of the docking results were produced using LigPlot.⁴³

2.3. Molecular Dynamics Simulation. MD simulations were carried out in two phases. In the first phase, the minimum energy conformation of CCR1 obtained from protein homology modeling process was employed as starting structure for MD simulation. In this phase components of simulation system included protein, lipid, and water molecules. In the second phase, output conformation resulted from the first phase of MD as well as the docked ligand were employed in MD process.

All of the MD simulations were carried out by the GROMACS 4 package⁴⁴ and in an explicit phospholipid bilayer. The gmx force field⁴⁵ was employed for the MD simulation of CCR1, while the lipid bilayer was described using a previously developed topology file (Tieleman, see <http://moose.bio.ucalgary.ca>).⁴⁶ This combination was employed effectively in many MD simulations studies of the interaction of various proteins and peptides with lipid bilayers, some were reviewed by Ash et al.⁴⁷ The protein was inserted at the center of the POPE bilayer with its long axis perpendicular to the membrane-water interface. The α -helical domain of the receptor was placed at the same level as the lipid bilayer, and overlappings between all of the molecules were discarded.

In the next step, water was added to fill in the gaps above and below the phospholipid leaflets and box edges, to hydrate the lipid head groups. Water molecules were represented applying a simple point charge (SPC) model. Solvent (i.e., water), ions, lipid, protein, and ligand were coupled separately to a temperature bath.

To balance the net charge associated with the presence of POPE, 5 water molecules were randomly replaced by Na^+ . This number of sodium ions must stay constant to preserve the electroneutrality of the investigated system. Final protein–lipid membrane system was placed in a box with the dimensions of $83 \times 82 \times 87$ (all in \AA) with a total of 43,616 atoms.

Periodic boundary conditions were applied in all three directions of space. Topology and coordinate of BX471 was generated by PRODRG.⁴⁸

After the starting system has been constructed, the system was energy minimized before the MD simulation using 200 steps of the steepest descent method in order to relax any steric conflicts generated during the setup.

An NVT ensemble was adopted at constant temperature of 310 K with a coupling constant of 0.1 ps and time duration of 100 ps. After stabilization of temperature, an NPT ensemble was performed. In this phase a constant pressure of 1 bar was employed with a coupling constant of 5.0 ps and time duration of 1 ns. NPT ensemble was finished after pressure stabilization. The coupling scheme of Berendsen was employed in both of NVT and NPT ensembles. The particle mesh Ewald (PME) method was used.⁴⁹ A 12 \AA cutoff for long-range and the Lincs algorithm for covalent bond constraints were applied.⁵⁰

In this configuration, the system was stable for 20 ns MD simulation. All the molecular images were produced using VMD.⁵¹ The trajectories were analyzed using the standard tools included in the GROMACS distribution. Time interval for *rmsd* calculation was 5 ps.

3. RESULTS AND DISCUSSION

3.1. Topology Prediction and Homology Modeling. All eleven techniques, explained in the Experimental Section, are aimed to recognize α -helices and to forecast the general topology of the protein in inside and outside of the biomembrane. All of these methods operate using different algorithms and predict different length and size of helices.

The final helices positions found in the developed CCR1 model showed that TM1 locates between amino acid number 38 to 60, TM2 between 71 to 91, TM3 between 109 to 135, TM4 between 147 to 170, TM5 between 203 to 226, TM6 between 238 to 264, and TM7 between 284 to 304 that are in agreement with most prediction data (Figure 1). The applied procedure employed here is much more robust, thanks to the use of multiple helices prediction that allows increasing the accuracy of the generated model. In the developed model, most transmembranes are at least 20 residues in length, quite compatible with the thickness of the hydrophobic region of the lipid bilayer. As expected, the generated model of CCR1 did not reveal major differences from the template protein when they were superimposed.

Model validation techniques check for whether a developed model satisfies standard steric and geometric criteria. Each of the methods applied in model building, template selection, sequence alignment, and refinement was subjected to its own internal measures of quality, but, finally the most significant criterion for the quality of generated 3D model of CCR1 is its conformational energy. The generated model of CCR1 was evaluated for stereochemical quality using the PROCHECK program. The aim of this test was to estimate how normal, or how unusual, the geometry of the residues in a given protein structure was, compared with the stereochemical parameters derived from well refined, high resolution structures.

Ramachandran plot, a plot of the $\varphi-\psi$ torsion angles for all residues in protein structure, is a significant factor in PROCHECK for evaluation of structures. A straightforward measure of quality of the generated 3D model that could be extracted from this plot was the percentage of residues in allowed regions to be

Table 2. Quality of CCR1 in Various Stages of Model Building Checked by PROCHECK

phase	region%				G-factor	
	favored	additional allowed	generously allowed	disallowed	dihedrals	overall
HM	87.1	10.4	1.5	0.9	-0.01	-0.10
phase I	75.8	21.8	1.2	1.2	-0.78	-0.80
phase II	71.2	22.7	2.8	3.4	-0.83	-0.82

very high (>90% residues).⁵² Another key feature in the structural evaluation is Goodness Factor or G-factor which indicates the quality of dihedral, covalent, and overall bond angles of the developed model. The overall value of this factor should be above -0.5 for a reliable model with the best model displaying values close to zero.

The final CCR1 model indicates that more than 97% of residue $\varphi-\psi$ angles are in the favored or additional allowed regions of Ramachandran plot (Table 2). With respect to Ramachandran plot, it is observed that only three residues (Arg335, Arg193, Glu272) are in a disallowed region. Residues located in the unfavorable regions are far from the substrate-binding domain, indicating that these residues may not affect the ligand–protein binding simulations.

In addition, the average G factor, the measure of the normality degree of the protein properties, was -0.1, which is inside the allowed values for homology models.

Regarding the main chain properties of the developed 3D structure of CCR1, neither significant bad contacts nor C_{α} tetrahedron distortion or hydrogen bond energy problems were seen.

Furthermore, the knowledge-based energy estimated by means of the PROSA-web⁵³ indicated that the generated model of CCR1 was well inside the range of a typical native structure⁵⁴ (Figure S3A).

Verify3D employs energetic and empirical techniques to generate averaged data points for each residue to evaluate the quality of extended model of protein. This score measures the compatibility of the generated model with its sequence by means of a scoring function. The compatibility score above zero in the Verify3D graph is corresponding to acceptable side-chain environments (Figure 4S). This suggests that the model has overall self-consistency in terms of sequence–structure compatibility.

3.2. Molecular Dynamics Simulation-Phase 1. Clarification of ligand binding mechanisms is the essential step to introduce more selective and potent lead compounds for a given target protein. To do this, we need to construct a 3D model of protein and then let it feel its natural environment. Molecular dynamic simulation is one of the best methods for such refinement. After obtaining a 3D structure of CCR1 to investigate the conformational variations of the protein within the hydrated lipid environment, the MD simulation for this model was performed in an explicit lipid bilayer environment. One of the most complicated difficulties, and yet also one of the most important tasks for any researcher in the field of molecular modeling, is to guarantee that an enough area of the potential energy hyper-surface of an explored system has been investigated by the MD simulation. In molecular levels, this means that all possible geometries of the investigated system should be searched in the MD simulation. Even with long time MD simulations process, this is only achievable for very small molecules with a few degrees of freedom. Systems with large number of atoms, of course, have exponentially greater numbers of possible geometries, many of

which are extremely energetically unstable. Nevertheless, raising the number of starting arrangements and systematically changing the position of those arrangements on the energy hypersurface permit us to investigate extensively all possible energetically acceptable geometries of the studied system. This has been implemented for the developed model of CCR1, by systematically changing the geometries of system and thus exploring all possible interactions between protein and its environment.

The POPE-CCR1 system remained firm after relaxation as a very slight drift in energy, temperature, or lipids density was monitored during the MD (data not shown). The stability of the simulated system was evaluated by calculating the root-mean-square deviation (flexibility) and radius of gyration (R_g).

Figure 2A shows the time history of $rmsd$ for backbone of protein structure immersed in lipid bilayer compared with the starting structure (the output of homology modeling). As has been seen, backbone $rmsd$ was about 4.7 Å after 20 ns of simulation and did not alter meaningfully after 2 ns of simulations. The $rmsd$ value implies that this protein structure has been affected by its environment. As it is indicated in this figure, the protein folding process shows good reliability since the structures of the developed model are stable during the MD simulation. Therefore, the used MD simulation was essential to specify geometry of CCR1 in vicinity of lipid bilayer.

To illustrate the secondary structure of CCR1, we used the DSSP program (<http://www.cmbi.kun.nl/gv/dssp/>) and the `do_dssp` program from the GROMACS package. The time evolution of the secondary structure for CCR1 is shown in Figure S5 in the Supporting Information.

As can be seen in this map, the seven TM segments of CCR1 maintained their α -helical secondary structure during the MD simulation. Together, results of $rmsd$ and secondary structure evaluation using DSSP, point out that the structure of CCR1 is stable during the course of the MD simulation.

The general alterations in the structure of simulated protein can be best visualized by studying the radius of gyration. Said another way, the radius of gyration of protein in the system is a criterion of the compactness of the protein arrangement and can be employed as a measure of protein aggregation during MD simulation. During the simulation of CCR1, there was a slow diminish of the gyration radius from around 2.3 nm down to around 2.2 nm (Figure S6). This compaction emerges to be a slow process and is attributed generally to the change of the interhelical angle between helices of the developed model.

After structural refinement of the CCR1 model by MD in phase I, the geometric quality determination of the backbone conformation, namely all tests performed in homology modeling step, was carried out again and the quality of the model was confirmed (for instance, results of PROCHECK are reported in Table 2).

The energy profiles for the 3D model of CCR1 after homology modeling and after MD simulation in phase I were compared

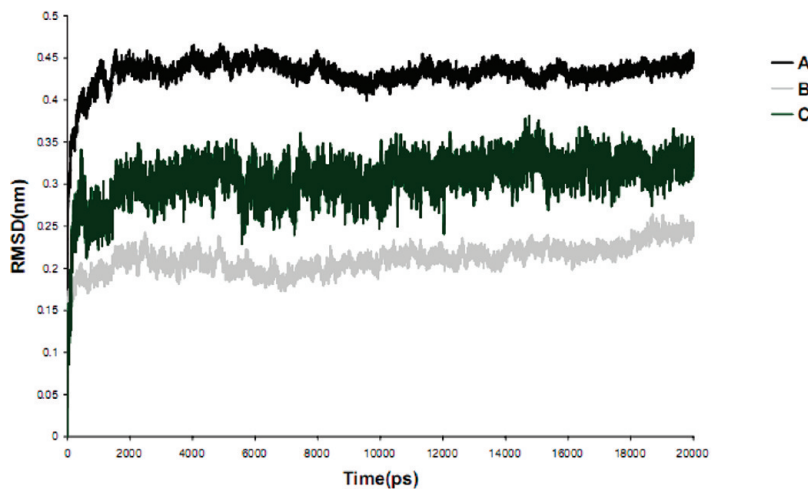


Figure 2. System stability was monitored as the backbone *rmsd* of CCR1 in (A) MD phase I and (B) MD phase II with respect to starting structures. Also, in (C) *rmsd* of ligand's atoms from the starting structure of docked ligand as a function of time during MD simulation phase II is shown.

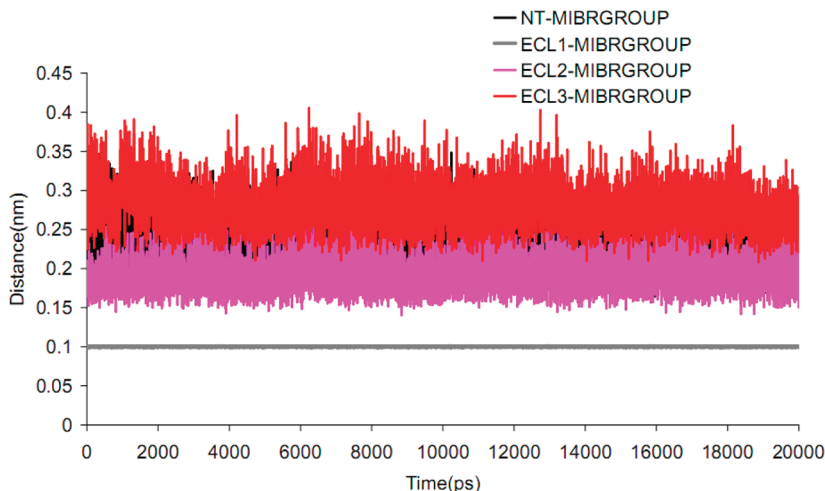


Figure 3. Time evolution of selected distances between various segments of CCR1. For more details refer to the manuscript.

using the ProSA score (Figure 3A and 3SB). This score assesses reasonable peptide fold geometry based on empirical mean force potentials. In the ProSA profile, residues with negative knowledge-based energy verify the reliability of the developed model. The ProSA score for the model after MD has a relatively better score than the HM model by decreasing the number of residues with positive knowledge-based energy.

Passing all checks by the developed model ensures that the extended CCR1 model will be able to describe various protein–ligand interactions and also the protein structure and function relationships.

3.2.1. Characterization of Extracellular Domains. Some studies by using experimental techniques on chemokine receptors have shown that extracellular segments are effectively involved in interaction with chemokines and natural ligands.^{55,56} Said another way, recent studies have revealed that the N terminus (NT) of chemokine receptors generally plays a crucial role for high affinity binding selectivity of natural ligands (RANTES and MIP-1 α), while ECL2 is important for natural ligands binding.^{57,58}

Therefore, the general tendencies in the dynamic behavior of the extracellular domain of CCR1 through MD simulation

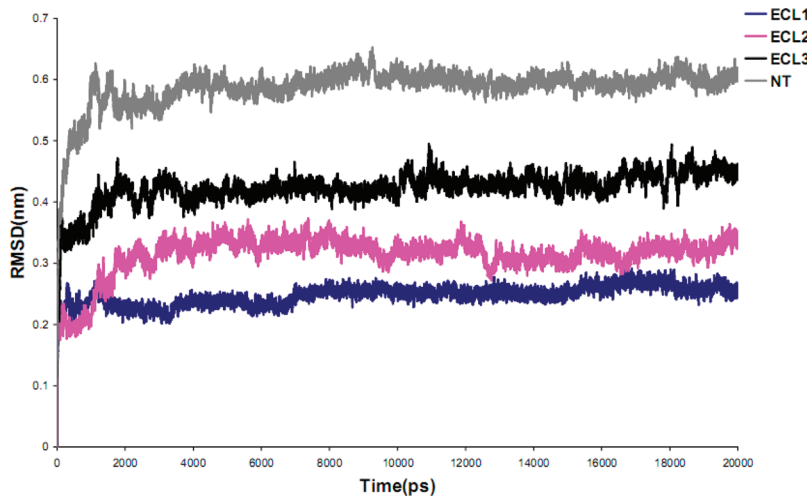
procedure were considered. In addition, CCR1 function was demonstrated considering the dynamic conformational character and structural flexibility of extracellular domain.

In CCR1, there are four extracellular and four intracellular segments, out of them there are six loop regions (ECL1, ECL2, ECL3, ICL1, ICL2, and ICL3). In addition to the loops in protein structure, there are two long segments in the N- and C-terminuses (NT and CT, respectively) that do not have any geometrical constraints. The initial structures of the N- and C-terminuses were built as an extended peptide chain conformation. Because in most GPCRs the ECL1 and ECL2 are linked via S–S bridge, a disulfide bond was introduced between CYS106 and CYS183.⁵⁹

It has been known that disulfide bond connecting the ECLs in chemokine receptors is essential for ligand binding.⁵⁶ The disulfide bond function has been assumed to maintain the structural integrity of the extracellular segments.⁵⁵ To further explore how the disulfide bond between CYS106 in ECL1 and CYS183 in ECL2 maintains such conformational integrity, the movement trajectories of extracellular segments of CCR1 were reconsidered. At first, the geometry center of the NT segment (1–37 residue) (Figure 1) was defined as a new group1 (NT), the

Table 3. Minimum, Maximum, Standard Deviation, and Range of Movements of Pseudo-Groups

movement type	standard deviation	min	max	range
NT-MIBRGROP	2.74 E-02	1.59 E-01	3.48 E-01	1.89 E-01
ECL1-MIBRGROP	4.11 E-04	9.87 E-02	1.01 E-01	2.54 E-03
ECL2-MIBRGROP	2.16 E-02	1.41 E-01	3.08 E-01	1.68 E-01
ECL3-MIBRGROP	2.75 E-02	2.08 E-01	4.13 E-01	2.04 E-01

**Figure 4.** Time dependence of the *rmsds* (Å) from starting structure for the backbone atoms of extracellular segments of CCR1 in the 20 ns MD simulation of phase I.

geometry center of the ECL1 segment (92–109 residue) was defined as the second group (ECL1), the geometry center of the ECL2 segment (171–202 residue) was defined as the third group (ECL2), the geometry center of the ECL3 segment (265–283 residue) was defined as the fourth group (ECL3), and the geometry center of membrane interface binding residues LEU40, PHE85, LEU109, SER165, LEU205, TYR255, and VAL288 was defined as another group (MIBRGROUP). Distances between these groups for the developed CCR1 model in the 20 ns MD simulation were calculated and shown in Figure 3, and also standard deviations, minimums, maximums, and ranges of movements are also reported in Table 3.

With respect to this figure and the range and standard deviation of movements, it can be found that the distance vibration amplitude of geometry center of NT segment from MIBRGROUP is wider than that of ECL1 and ECL2. As can be seen, in almost all of the MD time duration, the trajectory of NT stays on top of the trajectory of ECL1 and ECL2 segments. The top location of trajectories means that the NT segment is farther away from the cell membrane surface. It also implies that the motion range of ECL1 and ECL2 segments is restricted by the existing CYS106–CYS183 disulfide bond. These results allow us to explain the significances of the disulfide bond CYS106–CYS183 in maintaining the geometrical integrity of the extracellular domain of CCR1. To further assess the motion range of ECLs in developed CCR1, it can be seen in Figure 3 and Table 3 that the ECL3 shows the biggest vibration amplitude with a range of 2.04×10^{-1} nm, and ECL1 and ECL2 show a smaller vibration amplitude with a range of 2.54×10^{-3} and 1.68×10^{-1} , respectively, implying that ECL3 has the maximal and ECL1 has the minimal freedom of motion. The *rmsd* comparisons between corresponding backbones atoms of extracellular domain of

trajectories extracted from the 20 ns MD were carried out to further assess the geometrical flexibility of the extracellular regions (Figure 4).

For NT regions and ECL1–3 the *rmsd* value ranges are ~ 0 –0.60, ~ 0 –0.23, ~ 0 –0.32, and ~ 0 –0.42, respectively. The combination of the *rmsd* values and freedom of motion of the extracellular domain presented above reveals that ECL1 and NT region represent the most rigid and the most flexible extracellular regions of CCR1, respectively, and ECL3 is the most flexible loop among ECL1–3.

With respect to trajectories, it can be found that the extracellular domain of CCR1 formed a well-packed globular domain. Complex interactions including H-bond, electrostatic, and van der Waals contact occurred between extracellular segments in a majority of MD time duration. It could be seen that NT segment could stick out from this globular domain sometimes. Such globular shape domain was maintained during MD simulation by a complex interaction network formed by various bonds such as disulfide and hydrogen bonds, various forces such as van der Waals and columbic forces and salt bridges between extracellular segments. Obtained results for *rmsd* comparisons of various parts of extracellular domain indicate that NT and ECL3 are both of the most flexible segments in the CCR1 structure. On the other hand, solvent-accessible surface area was calculated for extracellular segments of CCR1 during 20 ns MD (data not shown). Results reveal that large numbers of residues in NT and ECL3 are exposed at receptor surface. Integrating these results with available experimental and theoretical data^{55–57} allows one to suggest a two-step ligand-binding mechanism: the NT first sticks out from the extracellular domain and accepts a suitable geometrical shape being ready to identify the ligand. Binding of ligand to NT causes the geometrical changes of this segment to facilitate the

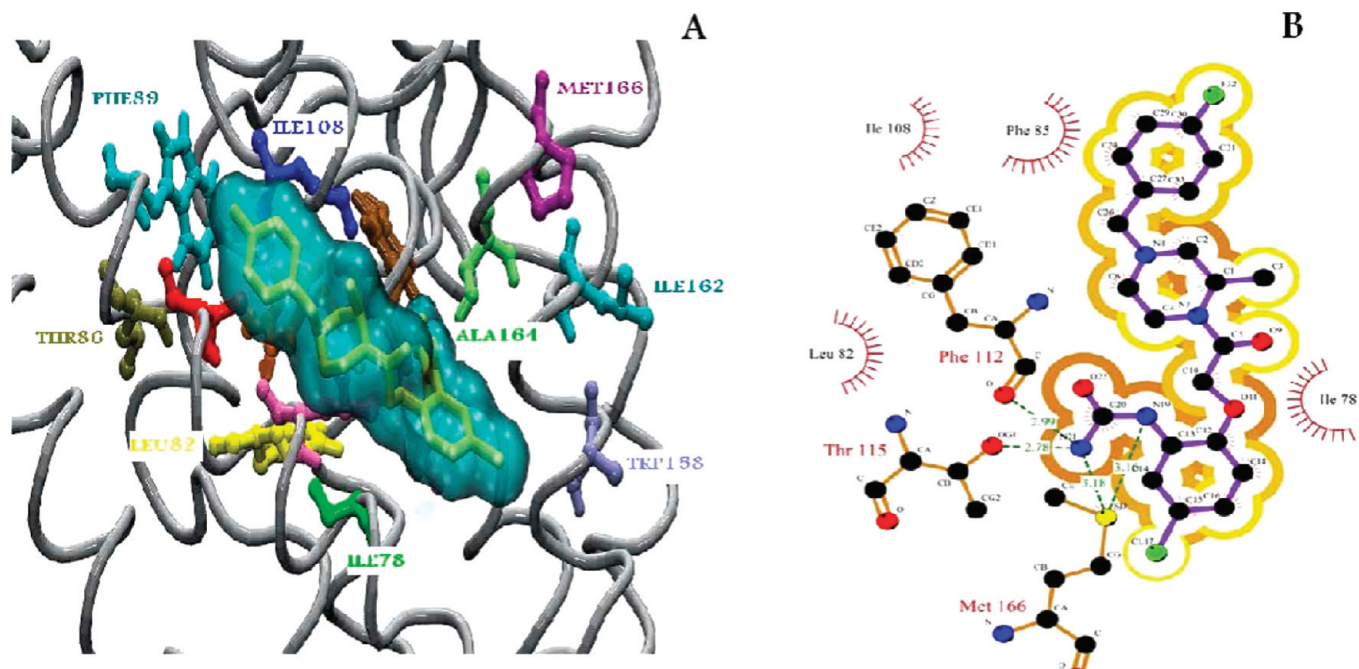


Figure 5. (A) 3D view of the predicted binding site of CCR1 by docking. BX471 represented as a yellow stick model inside a solvent excluded surface (SES) colored by a molecule. Important residues in the pocket are indicated by different colors. (B) Two-dimensional scheme of interactions between BX471 and CCR5 generated by LIGPLOT.

ligand interactions with ECL2 of CCR1. Finally, the interactions occurred between ECL2 and ligand which induce geometrical changes in CCR1 structure. These conformational changes bring the ligand closer to the binding pocket site of CCR2, and the interaction between the ligand and active site will be possible.

3.3. Docking. The molecular docking technique is the most common method for the estimation of protein–ligand interactions.

A putative binding pocket of CCR1 was determined according to the published results of experimental studies.^{60,61} The pocket is located in the extracellular side of the transmembrane domain (especially TM2 and TM3) and partly covered by the second extracellular loop (ECL2).

The 200 docking geometries for BX471 were separated into clusters according to *rmsd* tolerance (0.5 \AA) criterion. It means that in a cluster all conformations of BX471 mainly take a similar geometry. In addition to *rmsd* cluster analysis, AutoDock applies binding free energy evaluation to determine the best binding conformation. BX471 was successfully docked into the active site of CCR1, according to the docking protocol presented in the Method section.

Figure 5A,B gives the docking conformation of BX471 in the binding pocket. A careful inspection of the binding pocket indicated that BX471 adopted a position in a hydrophobic cage surrounded by Phe85, Ile108, Tyr113, Tyr114, Leu82, Tyr118, Phe122, and Ile78. As has just been reported, Tyr114 and Tyr113 are the key residues that construct the active pocket.⁶¹ It seems that the large effects of Tyr113 and Tyr114 on the binding of BX471 to the active site arise from the constructive van der Waals interactions between the phenyl rings of these residues and the piperazine ring of BX 471.

As shown in Figure 5A,B, there is an option for hydrogen bond formation between the urea nitrogen atom of BX471 and the oxygen atom of Thr115 or Phe112, with the bond lengths of

2.78 \AA and 2.99 \AA , respectively. This ensures that chlorobenzene ring can stably anchor into the hydrophobic pocket constructed by residues Phe112, Ile78, Leu 82, and Ser110. There is an additional probability for forming weak hydrogen bonds between BX471 and the sulfur atom of Met166, with the bond lengths of 3.18 \AA and 3.16 \AA , respectively.

The aromatic moieties of BX471 (fluorobenzene and chlorobenzene) form $\pi-\pi$ interaction with the side chains of the residues of Tyr113, Tyr114, and Tyr118. The chlorobenzene ring of BX471 was located between Tyr113, Tyr114, and Ile78. Also, it was observed that the fluorobenzene moiety of BX471 was positioned between Phe85, Thr86, and Ile106 in the substrate cavity space.

The chlorine atom of BX471 was extended away from the hydrophobic cage and was located between the residues Met166, Thr153, Trp 58, Ala164, and Ser165.

3.4. Molecular Dynamics Simulation-Phase II. To carry out an MD simulation course on a protein–ligand complex in a biological membrane system, one commonly employs available experimental data and computational manipulation to create a reasonable structure for the protein–ligand complex already bound to the biological membrane interface or inserted into the biological membrane interior.⁶² Following a suitable equilibration procedure on a given system consisted of a protein–ligand inserted in a biological membrane, a production simulation can be performed from which a researcher obtains information on the structure and dynamics of the studied system and its components. Due to existing limitations on simulation time lengths, the studied system is often unable to investigate the interactions significantly from the starting configuration, and therefore any bias in the starting geometries will affect the final results of MD simulation. To avoid this bias and make the comparisons to experimental conditions more meaningful, the MD simulation in phase I was carried out to obtain a stable and reliable starting

point. Another limitation in performing ideal MD simulations on these types of systems is the absence of enough information provided on the binding process itself. In an ideal world, a researcher would like to perform simulations in which the ligand is gradually approached into the binding pocket of the protein and to extract thermodynamic information on the binding process. Unhappily, the computational cost of such simulation procedures can become too expensive when full atomic details are considered. Therefore, as discussed above, we initially applied simple docking of the ligand to CCR1 to place the ligand into the active site. These results were not conclusive because *in vivo*, binding of inhibitor to a receptor is a dynamic process. Docking results can only stand for instantaneous states. Stable binding modes of ligand to receptor are valuable for further study. MD calculation will help choose stable binding structures and recognize the best binding mode. Therefore, one additional phase MD simulation was applied to gain further insight into the mechanism(s) that could explain the experimentally observed activity. Worthy of attention that what we can expect from molecular dynamics simulations of protein(s) in the presence of biological lipid bilayer is that such MD simulations give complete details of the motions of lipids, protein, and ligand(s) in the system. Through those information and statistical mechanics, thermodynamic properties could be estimated. Therefore, the CCR1-BX471 complex structure corresponding to the lowest calculated free energy of binding was selected for structure refinement using MD simulation.

3.4.1. Structural Fluctuations. The convergence of the system equilibrium was examined by following the time evolution of thermodynamic and structural quantities of the studied system during MD simulation. Protein total energy, root-mean-square deviation of the protein relative to the initial structure, the number of hydrogen bonds, and the solvent-accessible surface area as well as the overall secondary structure were monitored.

In Figure 2B, the time evolution of *rmsd* extracted from CCR1-ligand simulation is reported to check the stability of the simulation. *rmsd* approaches a constant value of $\sim 2.2 \text{ \AA}$ within 2 ns. In the last 18 ns simulation, the whole backbone of protein is fairly stable as indicated by the small magnitude of *rmsd* fluctuation of 0.3 \AA (Figure 2B). The simulation run could thus provide a suitable basis for the subsequent analyses. So, the average structure was obtained from the last 18 ns. After extraction, the average structure was compared with the docking structure.

To look at the fluctuation of the protein structure on a residue-by-residue basis, the time-averaged (last 5 ns of MD simulation) *rms* fluctuation (*RMSF*) of the peptidic backbone plus side chains (in black dashed) and the *RMSF* of the peptidic backbone (N, Ca, and C) (in solid gray) were depicted in Figure 6.

The averaging time period, 15 to 20 ns, was selected based on the observation of the *rmsd* drift of CCR1 during the MD simulation. Analysis of Figure 6 indicates that *RMSF* for CCR1 protein adopts the largest values at N-terminal and C-terminal regions. Such a large fluctuation value monitored for two terminuses is attributed to the existence of an unstructured free end consisting of residues 1 to 25 in NT and 320 to 355 in CT. The β -sheets and α -helices of CCR1 located in the central region of protein experience rather small fluctuations. This stable behavior of the β -sheets and α -helices of CCR1 is attributed to the network of hydrogen bonds stabilizing these secondary structures. It was discovered that during the dynamics simulations very few fluctuations gone beyond 0.2 \AA and even less fluctuations exceeded 0.25 \AA for the total protein. The precise

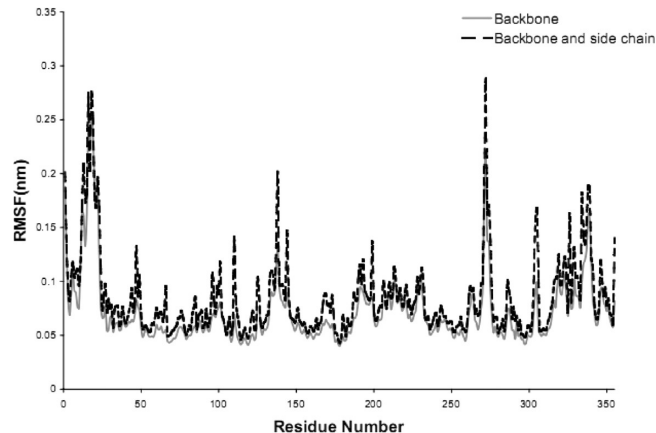


Figure 6. *rms* fluctuation (*RMSF*) of the peptidic backbone plus side chains (in black dashed) and the *RMSF* of the peptidic backbone (in solid gray) for CCR1.

study of Figure 6 shows that residues 133–145 with fluctuations between 0.09 to 0.2 \AA located close to the end of TM3 and beginning of ICL2 and residues 269–276 with fluctuations between 0.09 to 0.29 \AA located at the ECL3 have the highest fluctuation among the total residues in the central regions of protein. This result indicates once again that these regions of protein are more unstable than other regions during MD simulation.

A similar pattern emerges from the analysis of the secondary structures of the constituent helices of the 3D model as functions of time (Figure S8). In general, the 3D model of the CCR1 molecule retains a mostly 3D conformation throughout the MD simulation. During the 20 ns MD simulation, the 7 TMs are relatively stable, with only minor unfolding and refolding several times the helical structures. As can be seen, there are greater deviations from α -helicity, and from a fixed secondary structure, in the two terminuses, C-terminal and N-terminal segments, than in the central regions of protein. Also, it can be seen that the overall level of fluctuation in the secondary structure for residues 133–145 and residues 269–276 is higher than the other parts of the central regions of protein.

It can be seen that the CCR1–BX471 complex immersed among biomembrane and water molecules stays in equilibrium throughout the entire MD. Hence, we deduce that the MD simulation has constructed an improved and more relaxed structure of protein and ligand, which can be analyzed for further studies.

Importantly, simulation of CCR1 in the presence and the absence of ligand led to the different final peptide conformation and orientation. There are some differences in the backbone dihedral angle values, and these differences considerably affect the position of some residues in the Ramachandran plot. As it can be seen in Table 2, the presence of the ligand in the active site of protein during MD simulation leads to the displacement of some residues into the disallowed regions.

The *rmsd* of the ligand was calculated to obtain information on the position fluctuations and movements of ligand's atoms. Figure 2C shows that the *rmsd* of BX471 from the initial conformation increased to 0.34 \AA after 2 ns and then leveled off to the end of simulation. This shows that, after 2 ns simulation and preliminary fluctuations in the magnitude of *rmsd* of ligand's atoms, the ligand obtained an equilibrium state characterized by the *rmsd* profile.

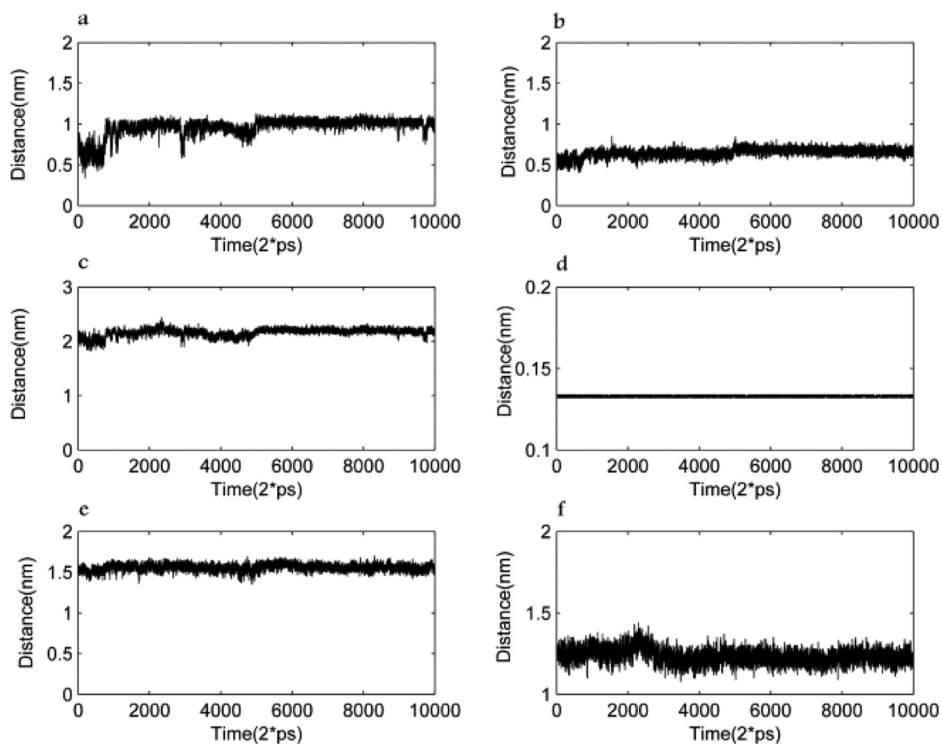


Figure 7. Time evolution of selected distances between residues involved in the inhibition reaction. The distances were extracted from a simulation of CCR1 in a complex with BX471 in phase II and include (a) Phe85-Phe112, (b) Phe85-Tyr113, (c) Phe85-Ile259, (d) Phe112-Tyr113, (e) Phe112-Ile259, and (f) Tyr113-Ile259.

3.4.2. Key Distance Fluctuations. Comparison of CCR1 structure in complex with BX471 after docking and after MD allowed for identification of the residues directly involved in binding of BX471 to CCR1. Within the CCR1 binding pocket, PHE85, PHE112, TYR113, and ILE259 are fully conserved after MD. Therefore, it could be deduced that CCR1-binding domain consists of at least the above-mentioned four residues. Among them, one residue, PHE85, belongs to the TM2, two residues (PHE112, TYR113) belong to the TM3, and the one residue, the ILE259, belongs to TM6 (Figure 1). The outstanding characteristic is that most of the residues presented in the CCR1 binding pocket are located within the well-defined secondary structures. The distances of the most important residues during the simulation that characterize the CCR1-binding site are pursued and reported in Figure 7. Analysis of the time-dependent fluctuation of the distances between the residues directly involved in creation of the CCR1-BX471 complex shows that the distances are fairly stable during the simulation time. Analysis of Figure 7 shows that distance fluctuations are within the range of ~ 0.1 nm.

Inhibitory reaction between protein and inhibitor depends on several factors including binding of the protein to the membrane surface, membrane properties, formation of the Michaelis–Menten complex, etc.^{63,64}

To occur the inhibitory reaction between CCR1 and BX471, a stable Michaelis–Menten complex has to form, which implies that distances stabilizing the ligand-protein complex are maintained.⁶⁵

We therefore monitored distances involving the inhibition reaction (BX471-PHE85, BX471-PHE112, BX471-TYR113, and BX471-ILE259) (Figure 8).

One can observe that time-dependent fluctuation of the distances between the residues in the active site and BX471 are

fairly stable during the simulation time. The results obtained also show that the shape of the CCR1-binding site stays practically constant during the MD simulation.

3.4.3. Binding Modes between BX471 and CCR1. Figure 9A depicts the binding conformation of BX471 in the binding pocket of CCR1, which were derived from the MD simulation followed by energy minimization.

The results obtained from our docking studies are supported by MD simulation in phase II for the CCR1–BX471 complex.

Importantly, as it can be seen in Figure 9, the presence of the ligand in the vicinity of protein during MD simulation leads to introduction of some new residues and some new interactions into the binding pocket compared with docking. There are some differences in key residues interacting with BX471, and these differences somewhat affect the position of BX471 in the binding pocket of CCR1.

BX471 adopts orientation whereby Phe112, Tyr113, and Tyr114 are involved in the stabilization of chlorobenzene ring and Phe85, Phe89, and Leu81 in the stabilization of fluorobenzene ring. On one end of BX471, the chlorobenzene ring is making π – π stacking interaction with TYR113 and TYR114 as is shown in Figure 9. Three criteria were employed to define a π – π stacking conformation. The distance of the two aromatic rings' geometrical centers should be < 6 Å. The angle between the planes of the two aromatic rings should be $< 45^\circ$. The angle between two vectors, one is the average of the two normal vectors to the two aromatic ring planes, the other is the coordinate vector of two aromatic ring geometric centers, should be $< 60^\circ$. The π – π stacking interaction between the chlorobenzene ring of BX471 and the aromatic ring of TYR113 satisfies all three criteria. The same interaction can be seen between the fluorobenzene ring of BX471 and the aromatic ring of PHE89. These interactions

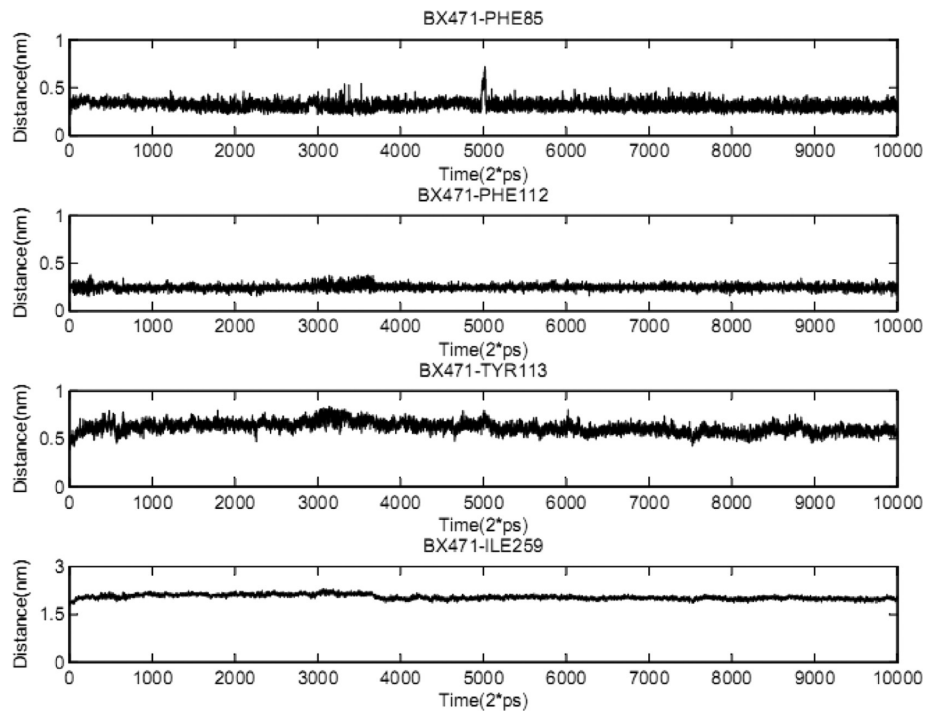


Figure 8. Time evolution of selected distances between residues that are interacting with the BX471. Distances are given in the individual panels. The distances were extracted from a simulation of CCR1 in the complex with BX471 in phase II.

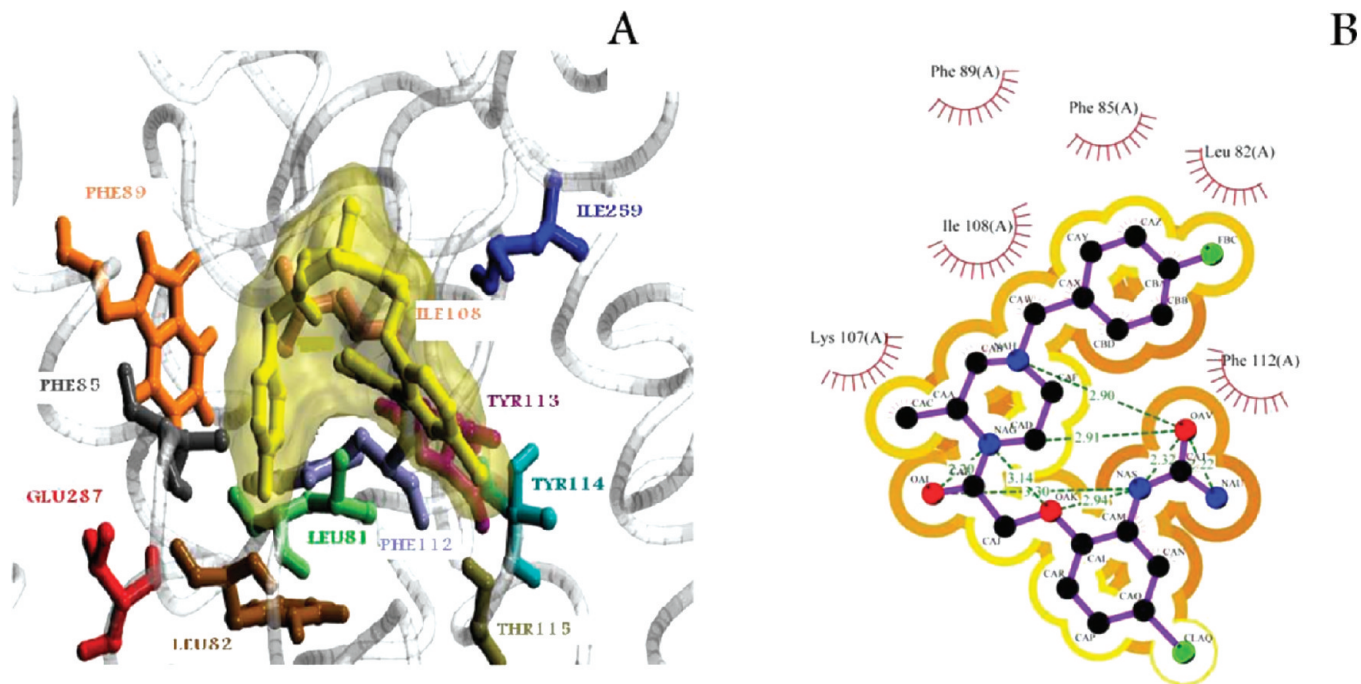


Figure 9. (A) The three-dimentional representation of interactions between BX471 and the CCR1 at the active site after MD simulation phase II and (B) schematic representation of the interaction between BX471 and the CCR1 produced using the Ligplot program.

are also observed in docking and well conserved in MD simulation confirming a crucial role of these interactions in ligand binding.

To further validate the developed model of interaction between BX471 and CCR1 active site, the software LIGPLOT was

used to investigate the hydrophobic and hydrogen bonding interactions. As shown in the 2D schematic interaction model of BX471 with CCR1 (Figure 9B), there are hydrophobic interactions between the Phe89, Phe85, Leu82, Lys107, and Ile108 and the carbon atoms of the fluorobenzene and the piperazine

rings of BX471, suggesting that more hydrophobic interactions around this area should improve CCR1 inhibitory activity.

Also, it must be noted that the conformation of BX471 in the CCR1 binding pocket becomes quite different from that in the docking binding pocket. The most important adjustment was to the dihedral angle between the fluorobenzene and the chlorobenzene rings. In the BX471–CCR1 complex after MD simulation, the fluorobenzene ring of BX471 becomes almost perpendicular to the chlorobenzene, whereas the relative position of these two rings in BX471 after docking was planar.

4. CONCLUSION

The lack of an experimentally determined 3D structure of the target protein often limits the application of structure-based drug development approaches. Homology modeling, combined with MD simulation, has been employed effectively for recognizing various characteristics of CCR1, a protein with no 3D structure. This developed model involves the main structural features of CCR1 protein according to the GPCRs characteristics and, therefore, could serve as a reliable target.

Docking simulations were carried out in order to predict the potential binding mechanism of BX471 to the generated CCR1. During the docking procedure a computationally derived CCR1 model was employed as a target molecule.

The obtained docking results for BX471 allowed us to propose a general binding mode of this ligand to CCR1 receptor and to determine residues involved in the ligand binding. For further investigation of binding mode of ligand and to explain the effects of ligand binding on protein conformation, we decided to perform a second molecular dynamics simulation on the BX471–protein complex in phase II of this study. CCR1 and its antagonist were investigated to get a full picture of the possible changes of the structure and binding mode during MD simulation. Results of MD simulation in phase II verified the stability of the docked complex presented in this research.

At the end of the MD simulation, a change in the position and orientation of the ligand in binding site was observed. This important observation indicated that the application of MD simulation after docking of ligands was useful. Explorative run of molecular dynamics simulation on the receptor–ligand complex revealed that except for Phe85, Phe112, Tyr113, and Ile259, the rest of the residues in the active site determined by docking more or less changed. It can be concluded that the unchanged residues could participate in the interaction of BX471 and CCR1 binding pocket. The binding model of BX471 shows clearly the mechanism of binding of this antagonist to CCR1. A detailed molecular level mechanism of CCR1 antagonistic action of BX471 has been described. Integrating results obtained in this study with available experimental data helps us to suggest a two-step ligand-binding mechanism: the NT first sticks out from the extracellular domain and accepts a suitable geometrical shape being ready to identify the ligand. Binding of ligand to NT causes the geometrical changes of this segment to facilitate the ligand interactions with ECL2 of CCR1. Finally, the interactions occurred between ECL2 and ligand induce geometrical changes in CCR1 structure. These conformational changes bring the ligand closer to the binding pocket site of CCR1, and the interaction between the ligand and active site will be possible.

The results of our combined modeling, dynamics, and docking studies can be utilized to generate potent CCR1 inhibitors to modulate CCR1 pathway in chronic inflammatory diseases.

■ ASSOCIATED CONTENT

S Supporting Information. Additional figures as noted in the text. This material is available free of charge via the Internet at <http://pubs.acs.org>.

■ AUTHOR INFORMATION

Corresponding Author

*Phone: +98 (311) 7922562. Fax: +98 (311) 6680011. E-mail: fassih@pharm.mui.ac.ir.

■ REFERENCES

- (1) Proudfoot, A. E. I. Chemokine receptors: multifaceted therapeutic targets. *Nat. Rev. Immunol.* **2002**, *2*, 106–115.
- (2) Godessart, N.; Kunkel, S. L. Chemokines in autoimmune disease. *Curr. Opin. Immunol.* **2001**, *13* (6), 670–675.
- (3) Karpus, W. J.; Kennedy, K. J. MIP-1alpha and MCP-1 differentially regulate acute and relapsing autoimmune encephalomyelitis as well as Th1/Th2 lymphocyte differentiation. *J. Leukocyte Biol.* **1997**, *62*, 681–687.
- (4) Gao, W.; Topham, P. S.; King, J. A.; Smiley, S. T.; Csizmadia, V.; Lu, B.; Gerard, C. J.; Hancock, W. W. Targeting of the chemokine receptor CCR1 suppresses development of acute and chronic cardiac allograft rejection. *J. Clin. Invest.* **2000**, *105*, 35–44.
- (5) Haringman, J. J.; Kraan, M. C.; Smeets, T. J. M.; Zwinderman, K. H.; Tak, P. P. Chemokine blockade and chronic inflammatory disease: proof of concept in patients with rheumatoid arthritis. *Ann. Rheum. Dis.* **2003**, *62*, 715–721.
- (6) Shahlaei, M.; Fassih, A.; Saghaie, L. Application of PC-ANN and PC-LS-SVM in QSAR of CCR1 antagonist compounds: A comparative study. *Eur. J. Med. Chem.* **2010**, *45*, 1572–1582.
- (7) Foord, S. M.; Bonner, T. I.; Neubig, R. R.; Rosser, E. M.; Pin, J.-P.; Davenport, A. P.; Spedding, M.; Harmar, A. J. International Union of Pharmacology. XLVI. G Protein-Coupled Receptor List. *Pharmacol. Rev.* **2005**, *57*, 279–288.
- (8) Wise, A.; Gearing, K.; Rees, S. Target validation of G-protein coupled receptors. *Drug Discovery Today* **2002**, *7* (4), 235–246.
- (9) Ivetac, A.; Sansom, M. Molecular dynamics simulations and membrane protein structure quality. *Eur. Biophys. J.* **2008**, *37*, 403–409.
- (10) Cherezov, V.; Rosenbaum, D. M.; Hanson, M. A.; Rasmussen, S. r. G. F.; Thian, F. S.; Kobilka, T. S.; Choi, H.-J.; Kuhn, P.; Weis, W. I.; Kobilka, B. K.; Stevens, R. C. High-Resolution Crystal Structure of an Engineered Human beta-Adrenergic G Protein Coupled Receptor. *Science* **2007**, *318*, 1258–1265.
- (11) Jaakola, V.-P.; Griffith, M. T.; Hanson, M. A.; Cherezov, V.; Chien, E. Y. T.; Lane, J. R.; Ijzerman, A. P.; Stevens, R. C. The 2.6 Angstrom Crystal Structure of a Human A2A Adenosine Receptor Bound to an Antagonist. *Science* **2008**, *322*, 1211–1217.
- (12) Okada, T.; Sugihara, M.; Bondar, A.-N.; Elstner, M.; Entel, P.; Buss, V. The Retinal Conformation and its Environment in Rhodopsin in Light of a New 2.2 Å Crystal Structure. *J. Mol. Biol.* **2004**, *342*, 571–583.
- (13) Warne, T.; Serrano-Vega, M. J.; Baker, J. G.; Moukhametzianov, R.; Edwards, P. C.; Henderson, R.; Leslie, A. G. W.; Tate, C. G.; Schertler, G. F. X. Structure of a [bgr]1-adrenergic G-protein-coupled receptor. *Nature* **2008**, *454*, 486–491.
- (14) Saghaie, L.; Shahlaei, M.; Fassih, A.; Madadkar-Sobhani, A.; Gholian, M.; Pourhossein, A. QSAR Analysis for Some Diaryl-substituted Pyrazoles as CCR2 Inhibitors by GA-Stepwise MLR. *Chem. Biol. Drug Des.* **2011**, *77*, 75–85.
- (15) Shahlaei, M.; Madadkar-Sobhani, A.; Mahnam, K.; Fassih, A.; Saghaie, L.; Mansourian, M. Homology modeling of human CCR5 and analysis of its binding properties through molecular docking and molecular dynamics simulation. *Biochim. Biophys. Acta, Biomembr.* **2011**, *1808*, 802–817.

- (16) Fu, W.; Cui, M.; Briggs, J. M.; Huang, X.; Xiong, B.; Zhang, Y.; Luo, X.; Shen, J.; Ji, R.; Jiang, H.; Chen, K. Brownian Dynamics Simulations of the Recognition of the Scorpion Toxin Maurotoxin with the Voltage-Gated Potassium Ion Channels. *Biophys. J.* **2002**, *83*, 2370–2385.
- (17) Wu, B.; Chien, E. Y. T.; Mol, C. D.; Fenalti, G.; Liu, W.; Katritch, V.; Abagyan, R.; Brooun, A.; Wells, P.; Bi, F. C.; Hamel, D. J.; Kuhn, P.; Handel, T. M.; Cherezov, V.; Stevens, R. C. Structures of the CXCR4 Chemokine GPCR with Small-Molecule and Cyclic Peptide Antagonists. *Science* **2010**, *330*, 1066–1071.
- (18) Ribeiro, S.; Horuk, R. The clinical potential of chemokine receptor antagonists. *Pharmacol. Ther.* **2005**, *107*, 44–58.
- (19) Liang, M.; Mallari, C.; Rosser, M.; Ng, H.; May, K.; Monahan, S.; Bauman, J.; Islam, I.; Ghannam, A.; Buckman, B.; Shaw, K.; Wei, G.; W, X.; Zhao, Z.; Ho, E.; Shen, J.; Oanh, H.; Subramanyam, B.; Vergona, R.; Taub, D.; Dunning, L.; Harvey, S.; Snider, R.; Hesselgesser, J.; Morrissey, M.; Perez, H. Identification and characterization of a potent, selective, and orally active. *J. Biol. Chem.* **2000**, *275*, 19000–19008.
- (20) Elices, M. BX-471 Berlex. *Curr. Opin. Invest. Drugs (BioMed Cent.)* **2002**, *3*, 865–869.
- (21) Kulagowski, J. J.; Broughton, H. B.; Curtis, N. R.; Mawer, I. M.; Ridgill, M. P.; Baker, R.; Emms, F.; Freedman, S. B.; Marwood, R.; Patel, S.; Patel, S.; Ragan, C. I.; Leeson, P. D. 3-[[(4–4-Chlorophenylpiperazine-1-yl)methyl]-1H-pyrrolo[2,3-b]pyridine: An Antagonist with High Affinity and Selectivity for the Human Dopamine D4 Receptor. *J. Med. Chem.* **1996**, *39*, 1941–1942.
- (22) Altschul, S.; Madden, T.; Schaffer, A.; Zhang, J.; Zhang, Z.; Miller, W.; Lipman, D. Gapped BLAST and PSI-BLAST: a new generation of protein database search programs. *Nucleic Acids Res.* **1997**, *25*, 3389–3402.
- (23) Chen, C.; Kernytsky, A.; Rost, B. Transmembrane helix predictions revisited. *Protein Sci.* **2002**, *11*, 2774–2791.
- (24) Tusnady, G.; Dosztányi, Z.; Simon, I. Transmembrane proteins in the Protein Data Bank: identification and classification. *Bioinformatics* **2004**, *20*, 2964–2972.
- (25) Cserzo, M.; Wallin, E.; Simon, I.; von Heijne, G.; Elofsson, A. Prediction of transmembrane alpha-helices in prokaryotic membrane proteins: the dense alignment surface method. *Protein Eng.* **1997**, *10*, 673–676.
- (26) Tusnady, G.; Simon, I. Principles governing amino acid composition of integral membrane proteins. *J. Mol. Biol.* **1998**, *283*, 489–506.
- (27) Hirokawa, T.; Boon-Chieng, S.; Mitaku, S. SOSUI: classification and secondary structure prediction system for membrane. *Bioinformatics* **1998**, *14*, 378–379.
- (28) Sonnhammer, E.; von Heijne, G.; Krogh, A. A hidden Markov model for predicting transmembrane helices in protein sequences. *Proc. Int. Conf. Intell. Syst. Mol. Biol.* **1998**, *6*, 175–182.
- (29) Kahsay, R.; Gao, G.; Liao, L. An improved hidden Markov model for transmembrane protein detection and topology. *Bioinformatics* **2005**, *21*, 1853–1558.
- (30) Hofmann, K.; Stoffel, W. TMbase - A database of membrane spanning proteins segments. *Biol. Chem. HoppeSeyler* **1993**, *347*, 166–170.
- (31) Juretic, D.; Lee, B.; Trinajstic, N.; Williams, R. Conformational preference functions for predicting helices in membrane proteins. *Biopolymers* **1993**, *33*, 255–273.
- (32) Adamczak, R.; Porollo, A.; Meller, J. Combining prediction of secondary structure and solvent accessibility in proteins. *Proteins* **2005**, *59*, 467–475.
- (33) Pollastri, G.; McLysaght, A. Porter: a new, accurate server for protein secondary structure prediction. *Bioinformatics* **2005**, *21*, 1719–1720.
- (34) Käll, L.; Krogh, A.; Sonnhammer, E. An HMM posterior decoder for sequence feature prediction that includes homology information. *Bioinformatics* **2005**, *1*, i251–257.
- (35) Neron, B.; Menager, H.; Maufrais, C.; Joly, N.; Maupetit, J.; Letort, S.; Carrere, S.; Tuffery, P.; Letondal, C. Mobyle: a new full web bioinformatics framework. *Bioinformatics* **2009**, *25*, 3005–3011.
- (36) Kabsch, W.; Sander, C. Dictionary of protein secondary structure - pattern-recognition of hydrogen-bonded and geometrical features. *Biopolymers* **1983**, *22*, 2577–2637.
- (37) Thompson, J.; Higgins, D.; Gibson, T.; CLUSTAL_W improving the sensitivity of progressive multiple sequence alignment. *Nucleic Acids Res.* **1994**, *22*, 4673–4680.
- (38) Baldwin, J.; Schertler, G.; Unger, V. An alpha-carbon template for the transmembrane helices in the rhodopsin family of. *J. Mol. Biol.* **1997**, *272*, 144–64.
- (39) Sali, A.; Blundell, T. Comparative protein modelling by satisfaction of spatial restraints. *J. Mol. Biol.* **1993**, *234*, 779–815.
- (40) Laskowski, R. A.; MacArthur, M. W.; Moss, D. S.; Thornton, J. M. PROCHECK: a program to check the stereochemical quality of protein structures. *J. Appl. Crystallogr.* **1993**, *26*, 283–291.
- (41) Luthy, R.; Bowie, J.; Eisenberg, D. Assessment of protein models with three-dimensional profiles. *Nature* **1992**, *356* (6364), 83–85.
- (42) Morris, G. M.; Goodsell, D. S.; Halliday, R. S.; Huey, R.; Hart, W. E.; Belew, R. K.; Olson, A. J. Automated docking using a Lamarckian genetic algorithm and an empirical binding free energy function. *J. Comput. Chem.* **1998**, *19*, 1639–1662.
- (43) Wallace, A. C.; Laskowski, R. A.; Thornton, J. M. LIGPLOT - A program to generate schematic diagrams of protein ligand interactions. *Protein Eng.* **1995**, *8*, 127–134.
- (44) Van Der Spoel, D.; Lindahl, E.; Hess, B.; Groenhof, G.; Mark, A. E.; Berendsen, H. J. C. GROMACS: Fast, flexible, and free. *J. Comput. Chem.* **2005**, *26*, 1701–1718.
- (45) Lindahl, E.; Hess, B.; van der Spoel, D. Gromacs 3.0: A package for molecular simulation and trajectory analysis. *J. Mol. Model.* **2001**, *7*, 306–331.
- (46) Tieleman, P.; MacCallum, J.; Ash, W.; Kandt, C.; Xu, Z.; Monticelli, L. Membrane protein simulations with a united-atom lipid and all-atom protein model: lipid–protein interactions, side chain transfer free energies and model proteins. *J. Phys.: Condens. Matter* **2006**, *18*, S1221–S1234.
- (47) Ash, W. L.; Zlomislic, M. R.; Oloo, E. O.; Tieleman, D. P. Computer simulations of membrane proteins. *Biochim. Biophys. Acta* **2004**, *1666*, 158–189.
- (48) Van Aalten, D. M.; Bywater, R.; Findlay, J. B.; Hendlich, M.; Hooft, R. W.; G., V. PRODRG, a program for generating molecular topologies and unique molecular descriptors from coordinates of small molecules. *J. Comput.-Aided Mol. Des.* **1996**, *10*, 255–262.
- (49) Darden, T.; York, D.; Pedersen, L. Particle mesh Ewald: An N [center-dot] logN method for Ewald sums in large systems. *J. Chem. Phys.* **1993**, *98*, 10089–10092.
- (50) Hess, B.; Bekker, H.; Berendsen, H. J. C.; Fraaije, J. G. E. M. LINCS: A linear constraint solver for molecular simulations. *J. Comput. Chem.* **1997**, *18* (12), 1463–1472.
- (51) Humphrey, W.; Dalke, A.; Schulten, K. VMD: Visual molecular dynamics. *J. Mol. Graphics* **1996**, *14*, 33–38.
- (52) Morris, A. L.; MacArthur, M. W.; Hutchinson, E. G.; Thornton, J. M. Stereochemical quality of protein structure coordinates. *Proteins* **1992**, *12*, 345–352.
- (53) Wiederstein, M.; Sippl, J. M. ProSA-web: interactive web service for the recognition of errors in three-dimensional structures of proteins. *Nucleic Acids Res.* **2007**, *35*, 407–410.
- (54) Wiederstein, M.; Lackner, P.; Kieberger, F. Direct in silico mutagenesis. In *Evolutionary Methods in Biotechnology*; Bräkmann, S., Schwienhorst, A., Eds.; Wiley-VCH: 2004.
- (55) Blanpain, C.; Lee, B.; Vakili, J.; Doranz, B. J.; Govaerts, C.; Migeotte, I.; Sharron, M.; Dupriez, V.; Vassart, G.; Doms, R. W.; Parmentier, M. Extracellular cysteines of CCR5 are required for chemokine binding, dispensable for HIV-1 coreceptor activity. *J. Biol. Chem.* **1999**, *274*, 18902–18908.
- (56) Genoud, S.; Kajumo, F.; Guo, Y.; Thompson, D.; Dragic, T. CCR5-Mediated human immunodeficiency virus entry depends on an amino-terminal. *J. Virol.* **1999**, *73*, 1645–1648.
- (57) Liu, S.; Shi, X.; Liu, C.; Sun, Z. Characterize dynamic conformational space of human CCR5 extracellular domain by molecular modeling and molecular dynamics simulation. *J. Mol. Struct.: THEOCHEM* **2004**, *673*, 133–143.

- (58) Pease, J. E.; Wang, J.; PD, P.; PM, M. The N-terminal extracellular segments of the chemokine receptors CCR1 and CCR3 are determinants for MIP-1 alpha and eotaxine binding, respectively, but a second domain is essential for efficient receptor activation. *J. Biol. Chem.* **1998**, *273*, 19972–19976.
- (59) Ji, T. H.; Grossmann, M.; Ji, I. G protein-coupled receptors. I. Diversity of receptor-ligand interactions. *J. Biol. Chem.* **1998**, *273*, 17299–17302.
- (60) de Mendonca, F. L.; da Fonseca, P. C.; Phillips, R. M.; Saldanha, J. W.; Williams, T. J.; Pease, J. E. Site-directed mutagenesis of CC chemokine receptor 1 reveals the mechanism of action of UCB 3562S, a small molecule chemokine receptor antagonist. *J. Biol. Chem.* **2005**, *280*, 4808–4816.
- (61) Vaidehi, N.; Schlyer, S.; Trabanino, R.; Floriano, W. B.; Abrol, R.; Sharma, S.; Kochanny, M.; Koovakat, S.; Dunning, L.; Liang, M.; Fox, J. M.; de Mendonca, F. L.; Pease, J. E.; Goddard, W. A.; Horuk, R. Predictions of CCR1 chemokine receptor structure and BX 471 antagonist binding. *J. Biol. Chem.* **2006**, *281*, 27613–27620.
- (62) Woolf, T. B.; Roux, B. Structure, energetics, and dynamics of lipid-protein interactions: A molecular dynamics study of the gramicidin A channel in a DMPC bilayer. *Proteins* **1996**, *24*, 92–114.
- (63) Peters, G. H. The dynamic response of a fungal lipase in the presence of charged surfactants. *Colloids Surf., B* **2002**, *26*, 84–101.
- (64) Peters, G. H. Computer imulations: a tool for investigating the function of complex biological macromolecules. In *Enzyme Functionality: Design, Engineering, and Screening*; Svendsen, A., Ed.; Marcel Dekker: New York, USA, 2004; pp 97–147.
- (65) Peters, G. H. Structure-based ligand design: from target protein to drug candidates. *Recent Res. Dev. Biophys.* **2004**, *3*, 501–526.